SCANNING X-RAY SCATTERING: EVALUATING THE NANOSTRUCTURE OF HUMAN TISSUES

Bert Müller[1,2], Hans Deyhle[1,2,3], David A. Bradley[4], Michael Farquharson[4], Georg Schulz[1], Magdalena Müller-Gerbl[5], and Oliver Bunk[3]

DOI 10.3884/0003.1.8

(peer-reviewed)

[1] Biomaterials Science Center, University of Basel, c/o University Hospital, 4031 Basel, Switzerland
[2] Materials Science Institute, Department of Dental Medicine, Hebelstrasse 3, 4056 Basel, Switzerland
[3] Paul Scherrer Institut, 5232 Villigen PSI, Switzerland
[4] Department of Physics, University of Surrey, Guildford, GU2 7XH, United Kingdom
[5] Institute of Anatomy, University of Basel, Pestalozzistr. 20, 4056 Basel, Switzerland

INTRODUCTION

In general, human tissue is organized in three-dimensional fashion and exhibits anisotropic properties that rely on its structure ranging from the atomic to the macroscopic level. While the anatomy describes the morphology and function of entire organs, the underlying processes on the cellular level are the focus of cell biology. Biochemistry concentrates on the molecular interactions.

Physicists are also fascinated by the human being but can only hardly contribute to the understanding of medical sciences. The exact description of complex structures comprising of a huge number of components is simply impossible. Note, the average human being in Switzerland is composed of 2.5×10^{27} atoms. Even the number of cells within such a person (10^{14}) is much larger than the number of stars within the Milky Way (3×10^{11}). Consequently, physicists are always impressed by the work of medical doctors. The medical doctors often come to decisions within seconds just looking at the patient asking a very few well-defined questions. Some of these medical doctors, however, need feedback from imaging facilities. Therefore, powerful radiology departments have been built up. Computed tomography, the facility with the best spatial resolution available for radiologists, reaches sub-millimeter resolution and therefore cannot provide images of individual cells within the human body. Only recently, micro computed tomography images obtained at synchrotron radiation facilities show individual cells of human tissue .

Images of cells are usually obtained by means of optical or sometimes electron microscopy. These data show a wealth of micro- and nanostructures, but are restricted to transparent tissues and surfaces. Surfaces, however, require expensive preparation procedures, which often result in substantial artifacts. Therefore, X-rays may be considered as the probe of choice to make visible morphological features within human tissues in a rather non-destructive way.

Since the real-space imaging using X-rays hardly reaches the nanometer scale, diffraction or scattering techniques are much better suited for the quantification of nanostructures. They yield exact mean values of the illuminated volume, which can be regarded as advantage. For the anisotropic and inhomogeneous human tissue, however, direct spatial resolution is highly desired. As a consequence, scanning along the specimen has been combined with the X-ray scattering methods. One distinguishes between wide-angle X-ray scattering (WAXS) for the analysis of the atomic structure and small-angle X-ray scattering for uncovering the nanostructure. Their combination with focused X-ray beams for scanning with true micrometer resolution requires high photon fluxes provided by synchrotron radiation sources and highly efficient and fast detection systems, which only became recently available.

The review demonstrates the power of scanning X-ray scattering for the visualization and quantification of the nanostructure in selected biological hard and soft tissues: tooth, bone, brain, and urethra, which goes beyond published work often related to bone and breast tissues in healthy and diseased states . The technique yields the abundance and orientation of all nanometer-sized organic and inorganic components within the X-ray beam focused to diameters in the micrometer range. The computer code for scattering data analysis is constantly developed and already reached a sophisticated level, which enables the suitable representation of X-ray absorption, abundance and orientation of nanometer-sized components with predefined length scale. These representations are easily readable for clinicians from different areas including dentistry and clearly reflect the tissue anisotropies usually related to the direction of growth and mechanical stimulation.

EXPERIMENTAL

X-rays that interact with matter are scattered and form patterns, which reflect the structure including the texture of the specimen. Experimentally, the scattered X-rays are recorded at the distance D_{sd}, whereby the through beam is covered by the beam stop (see Figure 1). This is necessary because the intensity of the through beam is much higher than the scattered portion of the X-rays. The pattern to be detected represents exact average values of the illuminated volume of the specimen. In order to obtain spatially resolved data, the specimen or the beam has to be moved in x-y-directions and a scattering pattern from each point has to be acquired for further analysis. To obtain the desired spatial resolution in real space, the monochromatic X-ray beam is often focused to micrometer size.

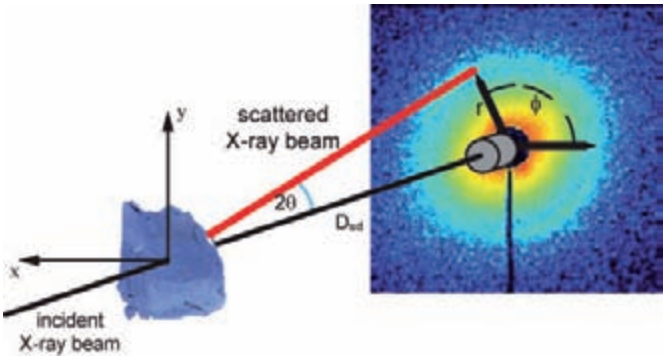

Figure 1: The X-ray beam of micrometer size hits a tissue slice - such as a histological section of the human thalamus - and forms a scattering pattern on the detection unit in distance D_{sd}. Scanning the tissue slice in micrometer steps in x-y directions, the patterns are recorded for subsequent evaluation.

The sizes of the periodic nanostructures within the specimen are inversely proportional to the scattering angle 2θ, given by the distance *r* from the through beam in the scattering pattern (see Figure 1). Therefore, two methods were introduced: small angle X-ray scattering (SAXS) with D_{sd} of several meters and wide angle X-ray scattering with rather short D_{sd}. SAXS serves for detecting nanometer-sized features between about 1 nm and 1 µm, whereas WAXS covers the scales below until the atomic distances are reached.

The total acquisition time for the scanning X-ray scattering measurements depends on the number of spots in the raster scan and the exposure time used. The latter in turn will depend on the scattering contrast in the specimen and the signal-to-noise ratio of the data desired. To give an example, one may raster scan a tissue specimen less than 100 µm thin in steps of 50 µm between adjacent spots and record thereby 40'000 patterns per square centimeter. At a data rate of 20 scattering patterns per second less than one hour is needed for

the data recording. In general, several samples can be mounted on the motorized holder to measure the specimens one-by-one in automatic way.

Solid specimens such as resin or paraffin embedded histological slices can be directly measured. Specimens in a wet environment (phosphate buffer saline or formalin solution) are hold in a polyimide sachet.

EVALUATION OF X-RAY SCATTERING PATTERN

Scanning SAXS and WAXS are raster scanning rather than full-field imaging techniques. This means, that each image is the result of a computerized analysis of typically several ten thousands of individual measurements.

Figure 2 shows a scattering pattern with many details obtained at the cSAXS beamline of the Swiss Light Source (Paul Scherrer Institut, Villigen, Switzerland). The ring structures are interrupted by the periphery of each module of the detection unit. Because of the symmetries in the pattern, however, the rings can be easily interpolated.

To quantify the acquired information, each of the thousands scattering patterns is divided in 16 radial segments around its center (see Figure 2 on the right). The integrated intensity of each segment at the pre-defined radius range is plotted as the function of the angular position (see red-colored data points in the graph of Figure 2). The symmetry-equivalent intensities from opposite segments are averaged. This means, one obtains eight values for the 16 segments. Approximating these eight values by means of a sine yields three parameters of interest. First, the abundance of nanostructures on a length scale range given by the radius range over which the intensity is integrated is derived from the offset I_{sym}. Second, the anisotropy of these nanostructures relates to the amplitude I_{asym}. Third, the phase shift of the sine determines the preferential orientation of the nanostructures. The three parameters are finally presented in the x-y-plane to be interpreted by the specimen suppliers. For the soft and hard human tissues, detailed anatomical knowledge is required to describe the features the medical experts are looking for.

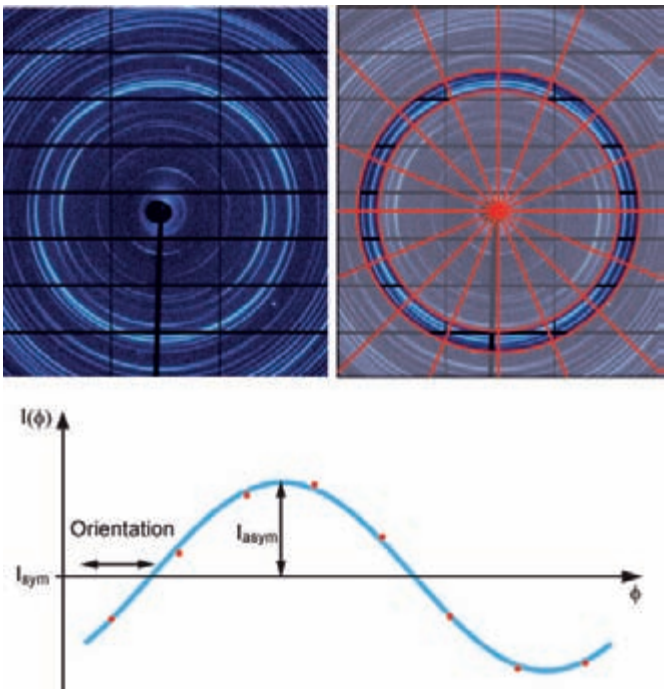

Figure 2: The scattered intensity is integrated along a ring around the central beam, divided in 16 segments. The intensity in each segment is plotted as angular position ϕ. The abundance of nanostructures is derived from the mean intensity of the ring I_{sym}. The anisotropy of the nanostructures relates to the amplitude I_{asym}. The phase shift of the sine determines the preferential orientation of the nanostructures along the X-ray beam.

EXAMPLE 1: BONY TISSUE OF THE FEMORAL HEAD

Scattering patterns of a section from the femoral head (see Figure 3) were acquired at a photon energy of 12.4 keV generated at the cSAXS beamline (Swiss Light Source, Paul Scherrer Institute, Villigen, Switzerland) with a sample-detector distance D_{sd} of 2.15 m. The specimen was scanned across the highly intense X-ray beam in 15 µm steps in x- and y-directions.

The representations of SAXS pattern of selected length scales properly demonstrate abundance and orientation of nanostructures at the periphery of the femoral head. The features on the selected length scales are predominately related to the cartilage anchored to the bone. Note, that the specimen originates from a decalcified, diseased human femoral head and thus mainly the collagen fiber orientations and abundances became to light. More detailed information on the nanostructures associated with the collagen fibrils of collagen-II at characteristic spacings of around 60 and 90 nm were published recently.

It became clear that from the surface of the articular cartilage towards the bone the orientation of the collagen-II fibers gradually changes from parallel to normal with respect to the joint surface, on the one hand, accommodating the gliding motion required of opposing articulating joint surfaces and, on the other hand, to accommodate the forces delivered onto the bone. A similar behavior of orientation changes for collagen-I prevalent in bone can be found below the cement line that is located at the cartilage-bone interface. Such orientational information from SAXS patterns illustrates loss of collagen organization as the result of articular cartilage degradation.

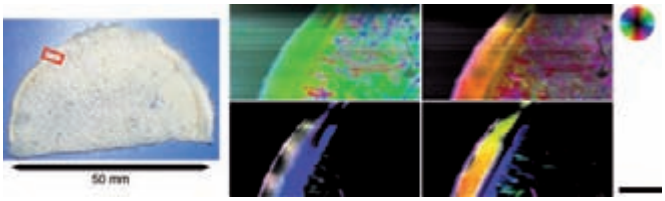

Figure 3**:** The image on the left shows a thin slice of a human femoral head, where the area for scanning X-ray scattering is marked. The image series on the right are representations of the SAXS patterns related to ranges from 1.6 to 1.7 nm (top, left), from 3.9 to 4.5 nm (top, right), from 12.5 to 13.7 nm (bottom, left) and from 20.2 to 23.1 nm (bottom, right), respectively. The colors are chosen according to the nanostructure's orientations, see color wheel, the brightness relates to the nanostructure's abundance. The bar corresponds to 1 mm.

EXAMPLE 2: HARD TISSUES OF THE HUMAN TOOTH

Human teeth are known as anisotropic hard tissues with strong preferential orientations on the micro- and nanometer scale. The directional ordering of the dentin and enamel nanostructures with respect to the tooth morphology, however, requires spatially resolved scattering data, which became available only recently . The high-resolution imaging facilities with several ten thousand megapixel-images, however, is only reached very recently .

Teeth are composed of the anisotropic natural materials dentin and enamel. Enamel is hard and brittle, composed mainly of densely packed calcium phosphates organized in prisms or rods with very few organic components. Dentin, also composed mainly of inorganic calcium phosphates, is interwoven by collagen-I, making it tougher and allowing it to absorb or redistribute mechanical stress. The combination of these two hard tissues forms a highly durable structure, which lasts a lifetime under extreme mechanical and chemical conditions in the oral cavity of the human being. Especially the dentin-enamel junction, the interface between dentin and enamel acts as a crack barrier, preventing cracks formed in the brittle enamel to propagate through the entire tooth .

SAXS experiments on human teeth slices were performed using a photon energy of 18.58 keV and a sample-detector distance of 7.14 m. The 500 µm-thin tooth slice, which was held between ap-

propriate polymer membranes to prevent dehydration, was scanned across the beam in 50 µm steps in x- and y-directions. This specimen was also measured in WAXS geometry with identical photon energy and step sizes, but with a sample-detector-distance of only 40.4 cm.

In the SAXS data, enamel yields scattering signals mainly parallel to the dentin-enamel junction, suggesting a perpendicular alignment of these nanostructures. The nanostructures in the dentin, however, lead to scattering signals normal to the dentin-enamel junction. The SAXS signals in enamel decrease with decreasing length ranges, almost disappearing below 10 nm (see Figures 4 and 5), which can be explained from the 15 nm-long rods in the enamel . At the length of a few nanometers and the sub-nanometer range, the differences in the chemical composition and structure between enamel and dentin become visible. Enamel maintains a highly oriented texture, while dentin structures can only be recognized for specific components (see Figure 5).

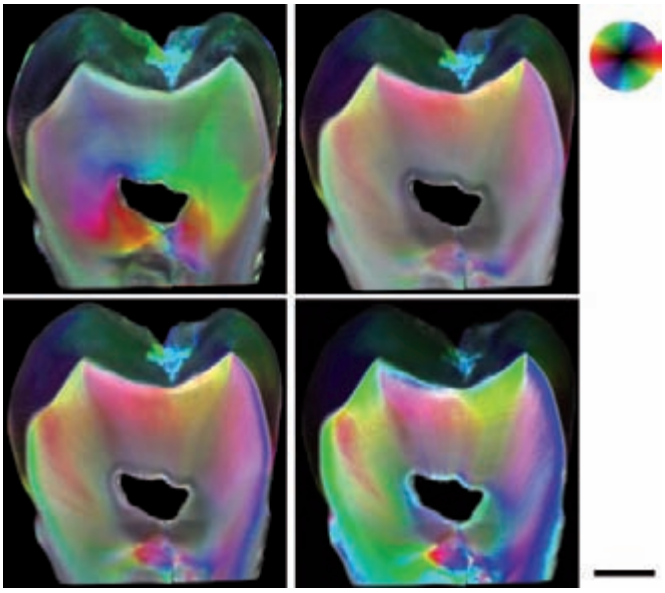

Figure 4**:** The hard tissue components of the human teeth with nanometer extensions show well-defined orientations. The nanostructures range from 185 to 231 nm (image top, left), from 53 to 71 nm (top right), 40 to 52 nm (bottom left), and 14 to 24 nm (bottom right). The colors are chosen according to the nanostructures orientations, see color wheel, their brightness relates to their abundance. The bar corresponds to 2 mm. The nanostructures in the dentin are nearly perpendicular to the dentin-enamel junction, whereas the ones of enamel are almost parallel to the dentin-enamel junction.

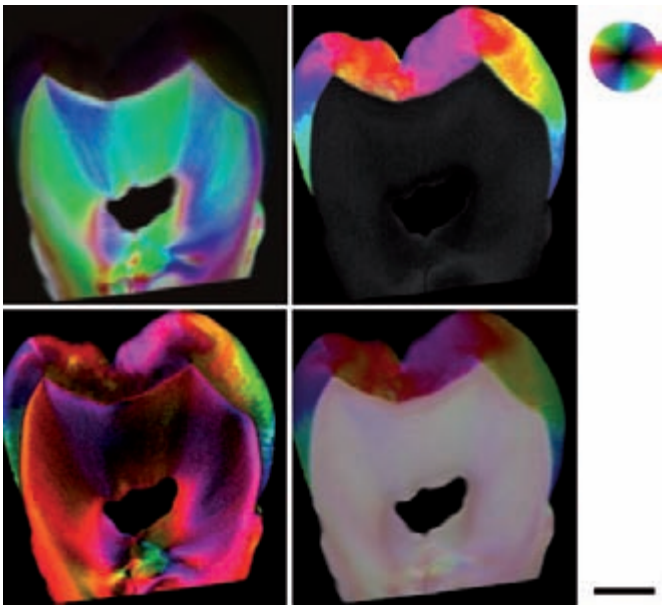

Figure 5: The scanning X-ray scattering to larger angles, represented by scanning WAXS, provides data on the molecular scales, which contain the structural and chemical composition of the tooth section. One clearly recognizes differences between the two kinds of hard tissue, i.e. dentin and enamel. Selecting certain scattering angles or lattice parameters, here 0.92 to 1.74 nm (image top, left), from 0.71 to 0.92 nm (top right), 0.40 to 0.53 nm (bottom left), and 0.22 to 0.24 nm (bottom right), the spatial distribution of the different components is uncovered. The colors are chosen according to the nanostructures orientations, see color wheel, their brightness relates to their abundance and the bar corresponds to 2 mm.

EXAMPLE 3: THALAMUS AS PART OF HUMAN BRAIN

The human brain is a prominent example for anisotropic and oriented soft tissue. SAXS pattern give rise to many details, which complement histology, since the periodicity of the nanostructures can be tracked deeply into the nanometer range as shown in the left image of Figure 6. Sophisticated analysis tools have to be developed to obtain an overview about all kinds of drawbacks and opportunities of SAXS pattern from differently stained and non-stained histological slices. Note, the potential influence of staining and embedding procedures can be studied, as the slices can even be investigated in wet state before the application of any preparation step.

The scanning X-ray scattering data shown were recorded at a photon energy of 11.2 keV and a specimen-detector distance of 7.1 m. The unstained thalamus slice, which was placed in a polyimide sachet, was scanned through the beam in steps of 100 µm in x- and y-directions with an acquisition rate of 5 images per second. It should be emphasized that the thalamus section scanned has centimeter extensions.

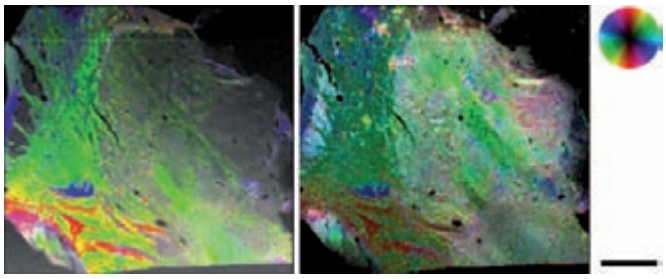

Figure 6**:** The human thalamus contains well-oriented nanostructures as shown by the two selected scanning SAXS images of a non-stained section prepared for histology. The left image represents the nanostructures from 4.6 to 6.3 nm and the right image shows the features of sizes from 161 to 185 nm. The orientation-dependent colors are according to the color wheel, their brightness is associated with their abundance. The bar corresponds to 5 mm.

EXAMPLE 4: URETHRA

The tissue of the human urethra resembles the porcine urethra . Figure 7 shows the scattering intensities of a 380 µm-thin section of an embedded porcine male urethra perpendicular to the symmetry axis. The images were generated with an 11.2 keV X-ray beam, scanned along the specimen in 50 µm and 75 µm steps in y- and x-direction, respectively.

The two main parts of the urethral tissue can also be distinguished in these SAXS images, which cover the entire nanometer range: the *tunica mucosa* in the central part surrounded by the *tunica muscularis*. The *tunica mucosa* consists of epithelium and the *lamina propria*. Epithelium is the innermost layer. The *lamina propria* is a loose tissue with abundant elastic networks. The *tunica muscularis* is composed of inner longitudinal and outer circular smooth muscles and an outermost ring of skeletal muscle fibers.

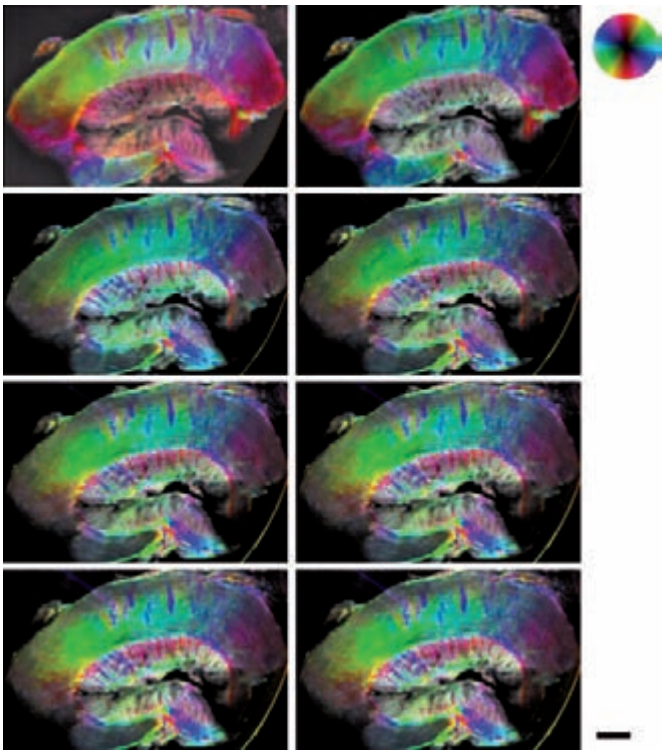

Figure 7: The series of scanning SAXS images shows the characteristic anatomy of the porcine urethra. The images from top-left to bottom-right represents the nanostructures ranging from 5 to 8 nm, 11 to 20 nm, 38 to 57 nm, 76 to 102 nm, 114 to 131 nm, 152 to 176 nm, 200 to 229 nm, and 269 to 305 nm, respectively. The colors are chosen according to the nanostructures orientations, see color wheel, their brightness relates to their abundance. The bar represents a length of 2 mm.

SUMMARY AND CONCLUSION

X-ray scattering techniques allow uncovering the nanostructure of human hard and soft tissues. They provide not only the presence of nanostructures but also their orientation and texture. The combination of these techniques with highly intense, focused X-ray, highly efficient and fast detection systems as well as scanning possibilities results in spatially resolved images, which are of high interest for medical experts in very different areas such as dentistry and urology. The Paul Scherrer Institute invites qualified applications from these experts for beamtime at the cSAXS beamline of the Swiss Light Source to extend the anatomical knowledge of human tissues on the entire nanometer scale.

ACKNOWLEDGEMENT

The valuable contributions of S. Buser, M. Imholz, A. Morel, and S. Mushkolaj, especially during the specimen preparation, are gratefully acknowledged.

REFERENCES

1. A. Lareida, F. Beckmann, A. Schrott-Fischer, R. Glueckert, W. Freysinger, and B. Müller, “High-resolution X-ray tomography of the human inner ear: Synchrotron radiation-based study of nerve fibre bundles, membranes and ganglion cells” Journal of Microscopy 234, 95-102 (2009).
2. O. Bunk, M. Bech, T. H. Jensen, R. Feidenhans’l, T. Binderup, A. Menzel, and F. Pfeiffer, “Multimodal x-ray scatter imaging” New Journal of Physics 11 (2009).
3. N. P. Camacho, S. Rinnerthaler, E. P. Paschalis, R. Mendelsohn, A. L. Boskey, and P. Fratzl, “Complementary information on bone ultrastructure from scanning small angle X-ray scattering and Fourier-transform infrared microspectroscopy” Bone 25, 287-293 (1999).
4. P. Fratzl, N. Fratzl-Zelman, K. Klaushofer, G. Vogl, and K. Koller, “Nucleation and growth of mineral crystals in bone studied by small-angle X-ray scattering” Calcified Tissue International 48, 407-413 (1991).
5. P. Fratzl, M. Groschner, G. Vogl, H. Plenk Jr, J. Eschberger, N. Fratzl-Zelman, K. Koller, and K. Klaushofer, “Mineral crystals in calcified tissues: A comparative study by SAXS” Journal of Bone and Mineral Research 7, 329-334 (1992).
6. S. Rinnerthaler, P. Roschger, H. F. Jakob, A. Nader, K. Klaushofer, and P. Fratzl, “Scanning small angle X-ray scattering analysis of human bone sections” Calcified Tissue International 64, 422-429 (1999).
7. V. Changizi, M. A. Oghabian, R. Speller, S. Sarkar, and A. A. Kheradmand, “Application of small angle x-ray scattering (SAXS) for differentiation between normal and cancerous breast tissue” International Journal of Medical Sciences 2, 118-121 (2005).
8. V. Changizi, S. Wilkinson, C. J. Hall, and G. Grossmann, “A study of the effect of formalin preservation on normal and cancerous breast tissues using small angle X-ray scattering (SAXS)” Radiation Physics and Chemistry 75, 932-935 (2006).
9. A. L. C. Conceicao, M. Antoniassi, and M. E. Poletti, “Analysis of breast cancer by small angle X-ray scattering (SAXS)” Analyst 134, 1077-1082 (2009).
10. A. L. C. Conceicao, M. Antoniassi, M. E. Poletti, and L. V. E. Caldas, “Preliminary study of human breast tissue using synchrotron radiation combining WAXS and SAXS techniques” Applied Radiation and Isotopes 68, 799-803 (2010).
11. M. Fernandez, H. Suhonen, J. Keyriläinen, A. Bravin, S. Fiedler, M. L. Karjalainen-Lindsberg, M. Leidenius, K. von Smitten, and P. Suortti, “USAXS and SAXS from cancer-bearing breast tissue samples” European Journal of Radiology 68, 89-94 (2008).
12. W. Kaabar, O. Gundogdu, A. Laklouk, O. Bunk, F. Pfeiffer, M. J. Farquharson, and D. A. Bradley, “μ-PIXE and SAXS studies at the bone-cartilage interface” Applied Radiation and Isotopes 68, 730-734 (2010).
13. K. K. W. Siu, S. M. Butler, T. Beveridge, J. E. Gillam, C. J. Hall, A. H. Kaye, R. A. Lewis, K. Mannan, G. McLoughlin, S. Pearson, A. R. Round, E. Schültke, G. I. Webb, and S. J. Wilkinson, “Identifying markers of pathology in SAXS data of malignant tissues of the brain” Nuclear Instruments and Methods in Physics Research, Section A: Accelerators, Spectrometers, Detectors and Associated Equipment 548, 140-146 (2005).
14. H. Deyhle, O. Bunk, S. Buser, G. Krastl, N. U. Zitzmann, B. Ilgenstein, F. Beckmann, F. Pfeiffer, R. Weiger, and B. Müller, “Bio-inspired dental fillings” in Proceedings of SPIE - The International Society for Optical Engineering Vol. 7401, 74010E (San Diego, CA, 2009).
15. J. H. Kinney, J. A. Pople, G. W. Marshall, and S. J. Marshall, “Collagen orientation and crystallite size in human dentin: A small angle X-ray scattering study” Calcified Tissue International 69, 31-37 (2001).
16. M. Al-Jawad, A. Steuwer, S. H. Kilcoyne, R. C. Shore, R. Cywinski, and D. J. Wood, “2D mapping of texture and lattice parameters of dental enamel” Biomaterials 28, 2908-2914 (2007).
17. V. Imbeni, J. J. Kruzic, G. W. Marshall, S. J. Marshall, and R. O. Ritchie, “The dentin-enamel junction and the fracture of human teeth” Nature Materials 4, 229-232 (2005).
18. A. Vieira, R. Hancock, H. Limeback, M. Schwartz, and M. Grynpas, “How does fluoride concentration in the tooth affect apatite crystal size?” Journal of Dental Research 82, 909-913 (2003).
19. F. Marti, T. Leippold, H. John, N. Blunschi, and B. Müller, “Optimization of the artificial urinary sphincter: Modelling and experimental validation” Physics in Medicine and Biology 51, 1361-1375 (2006).